pagepress

Journal of Agricultural Engineering

Journal of Agricultural Engineering 2026; LVII:1931
doi:10.4081/jae.2026.1931

Dynamic analysis and experimental study of sweet potato seedling transplanting mechanism with non-circular gear system *via* ADAMS-EDEM co-simulation

Bingliang Ye,[1,2,3] Hongbin Xue,[1] Gaohong Yu,[1,2,3] Yuxuan Ye,[1] Haili Zhou[1,2,3]

[1]School of Mechanical Engineering, Zhejiang Sci-Tech University, Hangzhou
[2]Provincial Key Laboratory of Agricultural Intelligent Sensing and Robotics of Zhejiang Province
[3]Key Laboratory of Agricultural Equipment for Hilly and Mountainous Areas in Southeastern China (Co-construction by Ministry and Province), Ministry of Agriculture and Rural Affairs, Hangzhou, China

Abstract

Soil resistance encountered by the sweet potato seedling transplanting mechanism during soil penetration is a critical factor influencing the dynamic characteristics of the mechanism. However, the intricate mechanism-soil interaction makes the fluctuation patterns of soil resistance analytically intractable. Therefore, this paper conducts a dynamic analysis and experimental research on the transplanting mechanism with the non-circular gear planetary train for sweet potato seedlings via ADAMS-EDEM co-simulation. ADAMS and EDEM software were used to establish simulation models of the sweet potato seedling transplanting mechanism and soil discrete element models, respectively, to conduct joint simulation analysis of the interaction process between the transplanting mechanism and the soil, obtaining the resistance and resistance torque curves exerted by the soil on the transplanting arm. A kineto-static analysis was employed to establish a dynamic model of the transplanting mechanism considering soil resistance, followed by an analysis to derive the loading and driving torque profiles for each component. A dedicated dynamic test bench was developed to conduct experimental evaluations and capture the dynamic characteristics of the prototype. The experimental dynamic curves exhibited high consistency with theoretical predictions in terms of mean, variance, and overall trends, validating the accuracy of the proposed model and analysis. This study integrates ADAMS-EDEM co-simulation into the dynamic analysis of a non-circular gear planetary transplanting mechanism for sweet potato seedlings. Unlike traditional research that treats soil resistance as a constant or simplified value, this work establishes the nonlinear, time-varying loading characteristics model during the soil-entry phase. By incorporating the simulated force and torque curves as direct inputs into the dynamic equations, this approach effectively resolves the discrepancy between external loads and actual working conditions inherent in previous models. The proposed approach offers a robust methodology for the dynamic modelling and analysis of complex soil-engaging mechanisms.

Key words: dynamic analysis; non-circular gear train; transplanting mechanism for sweet potato seeding; soil resistance; co-simulation; dynamic test.

Correspondence: Bingliang Ye, School of Mechanical Engineering, Zhejiang Sci-Tech University, Hangzhou 310018, China.
E-mail: zist_ybl@zstu.edu.cn

Introduction

The transplanting mechanism is the core component of the sweet potato seedling transplanting machine, and its level of development directly impacts the advancement and practical application of transplanting equipment technology. Based on the agronomic requirements of sweet potato seedling cultivation, domestic and international scholars have proposed chain-clamp-type and multi-rod-type transplanting mechanisms (Yan *et al*., 2022; Hui *et al*., 2023). The Agricultural Machinery Research Institute of Zhejiang Sci-Tech University, where the author works has developed a transplanting mechanism based on a modified elliptical gear planetary transmission system and has studied its kinematic characteristics and conducted transplanting experiments (Ye *et al*., 2016; Lu *et al*., 2016; Zhu *et al*., 2023). Based on the previous research, the present study performs a dynamic analysis and experimental investigation of the sweet potato seedling transplanting mechanism. This research provides both theoretical and experimental foundations for strength calculation, structural design, and dynamic performance optimization of the mechanism. Furthermore, it offers new insights into the dynamic behavior of soil-engaging mechanisms (Jin *et al*., 2025). Our research group has previously conducted dynamic analyses and experimental studies on double-arm mechanisms leveraging non-circular and double-arm incomplete gear planetary gear train vegetable plug seedling picking mechanisms (Ye *et al*., 2014, 2016, 2018; Zhou *et al*., 2025). These works provide a valuable reference for evaluating the dynamic performance of single-arm transplanting mechanisms. However, the operational schemes and agronomic requirements of the single-arm mechanism differ significantly from aforementioned designs, particularly during soil-engaging operations. The intricate interaction

between the arm and soil generates substantial resistance, which directly affects dynamic performance (Rajendran and Ranganathan, 2025). Furthermore, due to the nonlinearity and variability of this interaction, soil resistance is difficult to model accurately, and its variation patterns remain challenging to analyze. This study establishes an ADAMS-EDEM co-simulation model of the transplanting mechanism and conducts joint simulations to obtain the soil resistance experienced during transplanting operations (Li *et al*., 2023; Li *et al*., 2022). Based on the simulation results, a dynamic model of the mechanism is developed and analysed. Finally, dynamic testing of the prototype is performed to extract the dynamic characteristics and verify the accuracy of the theoretical model and simulation results (Shi *et al*., 2024).

Materials and Methods

Working principle of the transplanting mechanism

Figure 1 illustrates the transplanting procedure for sweet potato seedlings. Sweet potato seedlings are manually placed into the clips of the intermittent synchronous belt feeder 3. The gripping claws of transplanting arm grips a seedling at the pick-up point J, moves through point F, and inserts it into the soil. and then quickly opens to release them at the transplanting point G, completing one transplant cycle. The trajectory of the arm tip follows the path J-F-G. Subsequently, the mechanism returns to its initial configuration to prepare for the succeeding cycle.

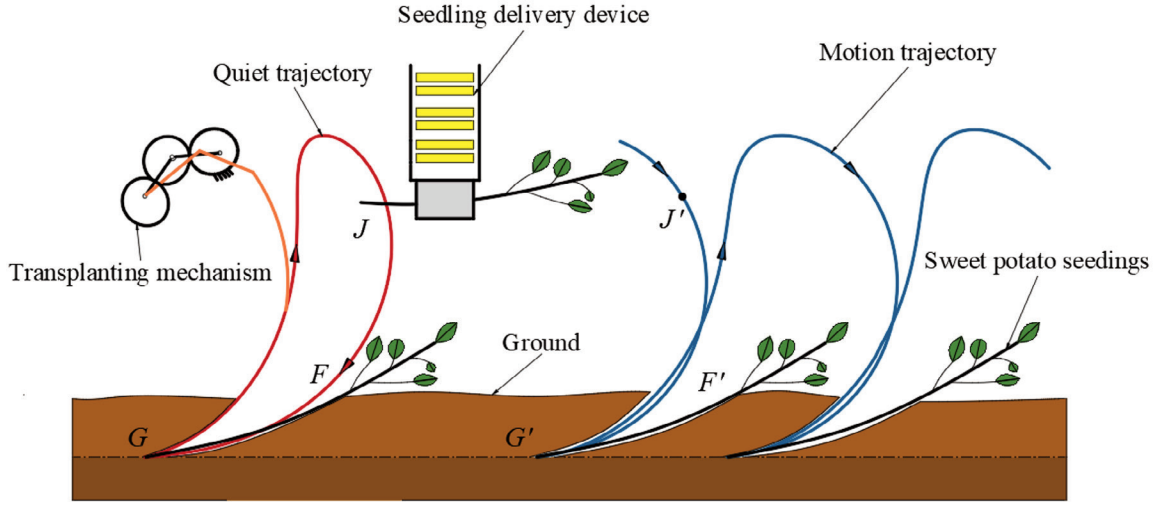

Figure 1. Sweet potato seedling transplanting plan.

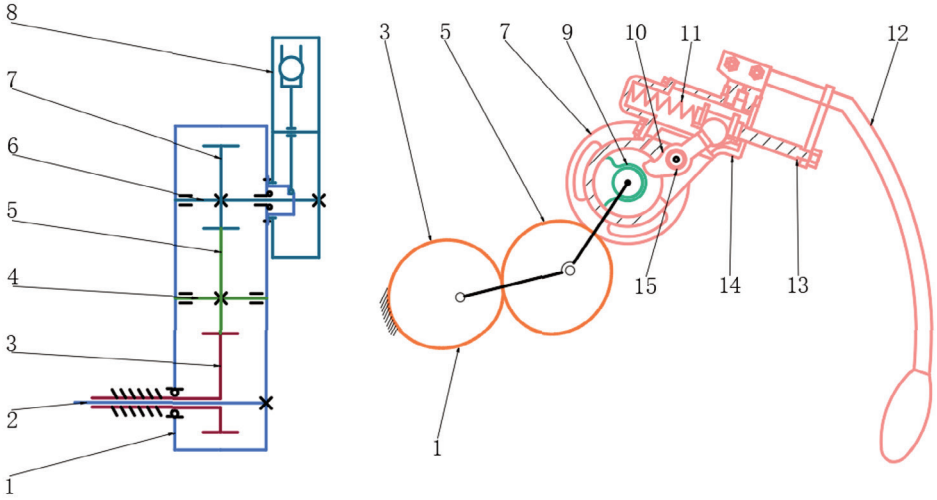

Figure 2. Schematic diagram of the sweet potato seedling transplanting mechanism with a modified elliptical gear planetary transmission system. 1. Gearbox housing (planetary carrier). 2. Drive shaft. 3. Sun gear. 4. Intermediate shaft. 5. Intermediate gear. 6. Planetary shaft. 7. Planetary gear. 8. Transplanting arm. 9. Cam. 10. Fork. 11. Spring. 12. Gripping claws. 13. Push rod. 14. Transplanting arm housing. 15. Fork shaft.

The modified elliptical gear planetary transmission system used in the sweet potato seedling transplanting mechanism consists of a planetary gear system and a transplanting arm, as shown in Figure 2. The planetary gear system includes three modified elliptical gears: the sun gear 3, intermediate gear 5, and planetary gear 7. The sun gear 3 is fixed to the machine frame by a flange, while the gearbox housing 1 is securely connected to the driving shaft 2. The intermediate gear 5 meshes with both the sun gear 3 and the planetary gear 7. The transplanting arm comprises the housing 14, cam 9, fork 10, gripping claws12, and push rod 13. The transplanting arm housing 14 is firmly attached to the planetary gear shaft 6, and the cam 9 is securely mounted on the gearbox housing 1.

During operation, the driving shaft 2 drives the gearbox housing 1 to rotate clockwise at a constant speed. Through the transmission of the planetary gear train, the planet gear and the rigidly attached transplanting arm housing 14 revolve with the housing while simultaneously rotating counterclockwise at a variable speed about the planet gear shaft 6. Meanwhile, the cam 9 fixed to the gearbox housing actuates the fork 10, which, in cooperation with the spring 11, drives the push rod 13 in reciprocating motion to control the opening and closing of the gripping claws 12. The operating process is divided into four stages: seedling pick-up, transfer, transplanting, and return, with the corresponding planetary carrier rotation angle ranges shown in Figure 3.

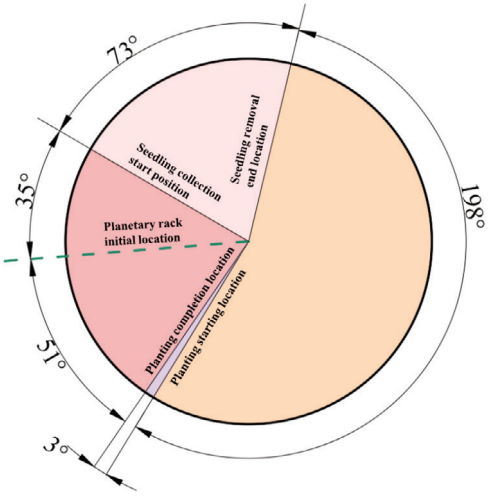

Figure 3. Working cycle diagram of the transplanting mechanism.

Soil resistance analysis *via* ADAMS-EDEM co-simulation

During the transplanting operation, the soil exerts resistance on the transplanting arm of the sweet potato seedling transplanting mechanism. Therefore, to ensure the dynamic model aligns with actual working conditions, this study leverages ADAMS-EDEM co-simulation to characterize the interaction between the arm and the soil (Shao, *et al*., 2023). The ADAMS post processing module generates the force and torque curves exerted by the soil on the transplanting arm, allowing for an analysis of the variation pattern of soil resistance throughout the transplanting cycle. These extracted data serve as a critical basis for the subsequent dynamic analysis of the mechanism.

Transplanting mechanism simulation model

A three-dimensional model of the sweet potato seedling transplanting mechanism was constructed using SolidWorks and subsequently imported into ADAMS software. Material properties were defined for each component, and global gravity was applied. Appropriate kinematic pairs were established between the relevant components, and a rotational drive of 240 r/min was applied to the revolute joint between the planetary carrier and the machine frame (Issa *et al*., 2020). To enable real-time transmission of the transplanting mechanism's motion state to EDEM and real-time feedback of the force conditions on the transplanting arm to ADAMS, a general force vector (GFORCE) aligned with the global coordinate system was applied at the center of mass of each of the four key components: the intermediate gear, planetary gear, planetary carrier, and transplanting arm. The user-defined parameter was set to 0.0, and the program function was specified as ACSI_Adams. The solution IDs were assigned as 1, 2, 3, and 4, respectively. The resulting ADAMS simulation model of the transplanting mechanism is shown in Figure 4.

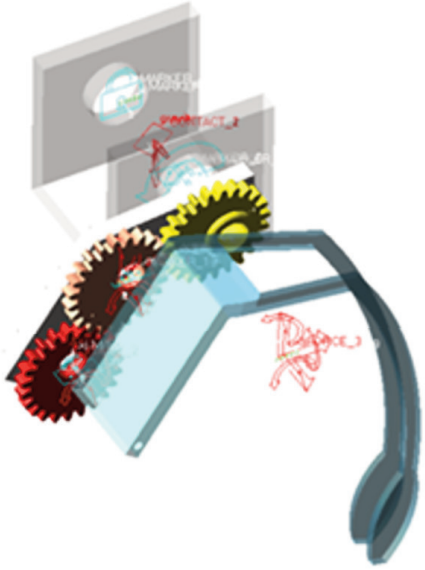

Figure 4. ADAMS simulation model of the transplanting mechanism.

Soil discrete element model

Soil contact force model

In discrete element method (EDEM) simulations, the Hertz-

Figure 5. Soil angle of repose test.

Mindlin with JKR contact model combines Hertzian contact theory with the Mindlin-Deresiewicz tangential force model and incorporates the JKR surface energy parameter to simulate adhesive forces between particles (Walunj *et al*., 2023). This model effectively captures the influence of cohesive forces between moist particles on their motion behavior. Therefore, we employed the Hertz–Mindlin with JKR contact model to establish a discrete element model of sweet potato transplanting soil. Soil parameters were defined based on relevant literature (Li *et al*., 2022; Guo and Huihuang, 2023), as shown in *Table S1*.

Calibration of the soil surface energy parameters

Soil surface energy parameters are key indicators in discrete element modeling. To ensure that the simulated soil particles closely resemble those found in actual sweet potato cultivation soil, these parameters were calibrated through a combination of soil angle of repose experiments and corresponding simulation-based angle of repose tests (Ye *et al*., 2024). As shown in Figure 5, an iron plate was first used to block the outlet at the bottom of the funnel. An appropriate amount of sweet potato seedling planting soil was then poured into the funnel. Afterwards, the iron plate was swiftly removed, allowing the soil to form a conical pile in the collection tray. The angle of repose was measured using an electronic protractor (Xue *et al*., 2022; Yu, 2023). This experiment was repeated ten times, yielding angles of repose of 38.81°, 39.63°, 38.85°, 39.15°, 38.73°, 38.96°, 37.92°, 38.51°, 38.49°, and 39.54°, with an average value of 38.86°.

The simulation of the angle of repose tests was using an integrated Hertzian contact model (HSCM) and a linear cohesion model (LCM). Soil particles were randomly generated above the funnel opening, with particle parameters set according to the data in Table S1. The soil surface energy parameters were set to 0 J/m², 1.5 J/m², and 3 J/m², and three corresponding simulation trials were performed. Each simulation concluded once all generated particles had fallen through the funnel and come to rest (Zhang *et al*., 2022). The simulation results are shown in Figure 6. Using the protractor and clipping tools in the EDEM analyst, the angle of repose was measured from the *x*- and *y*-directions of the conical surface (Jun, 2024). The simulated angles of repose under different surface energy parameters are shown in *Table S2*.

When the surface energy parameter is set to 0 J/m², the soil exhibits the smallest angle of repose, characterized by weak particle cohesion and a loose structure. Conversely, at a surface energy parameter of 3 J/m², the angle of repose reaches its maximum, indicating strong cohesion between particles and poor flowability. These results demonstrate a positive correlation between the surface energy parameter and both the inter-particle cohesion and the resulting angle of repose. Based on this relationship, the surface energy parameter was calibrated to 1.43 J/m², yielding a simulated angle of repose of 39.12°, which closely matches the experimental value of 38.86°. Therefore, the optimal surface energy parameter for the soil is determined to be 1.43 J/m².

ADAMS-EDAM co-simulation

A discrete element simulation model was established, as shown in Figure 7. The Hertz-Mindlin with JKR contact model was selected to represent particle interactions, with the particle surface energy parameter set to 1.43 J/m². A rectangular container measuring 500 mm in length, 100 mm in width, and 150 mm in height was constructed, and a particle factory was placed above it. Particle parameters were assigned according to *Table S1*. Subsequently, the particle bed model was generated, and the transplanting mechanism model was imported with defined material properties for its components (Lai *et al*., 2019). Finally, the coefficients of static friction, kinetic friction, and restitution between the soil and the transplanting arm were set to 0.5, 0.3, and 0.5, respectively (Massah *et al*., 2021).

An ADAMS–EDEM co-simulation analysis was conducted. The co-simulation interface in EDEM was enabled, and the corresponding .cosim file was imported into ADAMS for co-simulation (Sanborn *et al*., 2023). The interaction between the transplanting arm and the soil, as well as the disturbance of soil particles, was observed within the EDEM interface for planetary carrier angles ranging from 216° to 339°,as shown in Figure 8. The generated simulation result file was imported into the ADAMS post-processing module, Since the transplanting arm housing is rigidly connected to the planetary gear shaft, forces acting on the planetary gear rotational joint were measured. This yielded force and torque variation curves exerted by the soil on the transplanting arm, as shown in Figure 9.

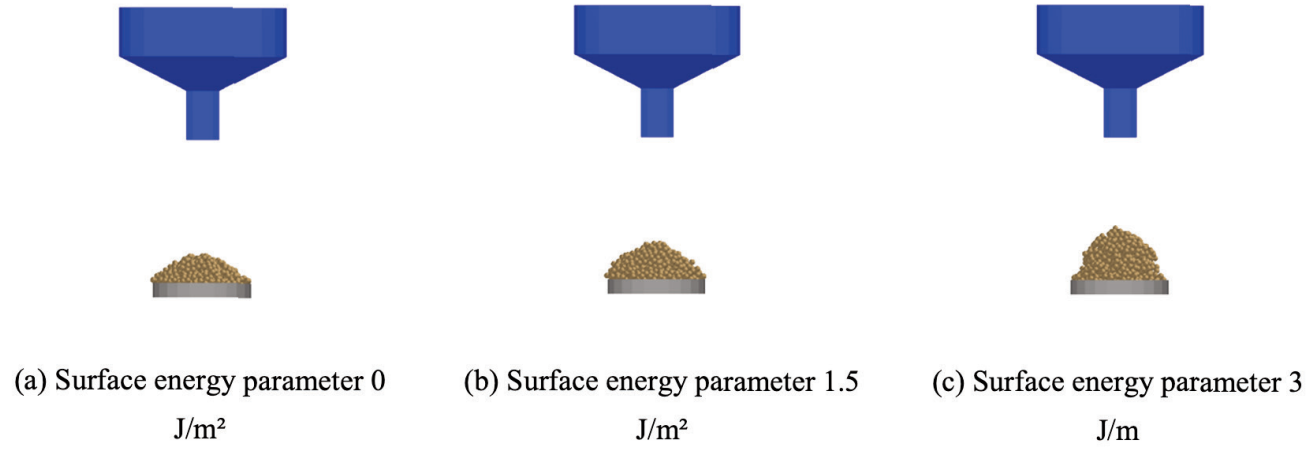

Figure 6. Soil angle of repose simulation experiment.

Figures 8 and 9 illustrate that when the planetary carrier angle is between 216° and 339°, the transplanting arm is subjected to soil resistance. At 216°, the transplanting arm begins to penetrate the soil, and both the soil resistance and torque gradually increase as the planetary carrier continues to rotate (Sun *et al*., 2025). When the planetary carrier angle reaches 251°, the soil resistance in the *y*-direction acting on the transplanting arm attains its maximum value of –12.56 N. At 291°, the soil resistance in the *x*-direction and the torque reach their respective maxima of –16.69 N and –2.774 N·m. As the planetary carrier rotates further, the transplanting arm starts to withdraw from the soil, resulting in a decrease in both soilresistance and torque. At 310°, the transplanting arm experiences downward soil pressure, causing a reversal in the direction of the force in the *y*-direction. When the planetary carrier angle reaches 340°, the transplanting arm is fully withdrawn from the soil, and both soil resistance and soil torque return to zero (Zhou *et al*., 2022). The curves depicting soil resistance and torque as a function of planetary frame rotation angle, obtained through ADAMS-EDEM co-simulation, accurately characterise the nonlinear load behaviour of the transplanting arm during the soil entry, soil engagement, and soil exit phases. These soil resistance and moments are incorporated as external load terms within the transplanting mechanism's dynamic equations. This enables the established dynamic model to account for soil interactions during actual planting operations, thereby enhancing the accuracy and engineering applicability of the dynamic analysis results.

Dynamic analysis of transplanting mechanisms

Transplanting mechanism dynamics modelling

Dynamic modelling of planetary gears

To ensure the dynamic model of the planetary gear (including the transplanting arm) closely reflects actual operating conditions, the soil entry phase of the transplanting arm -corresponding to a

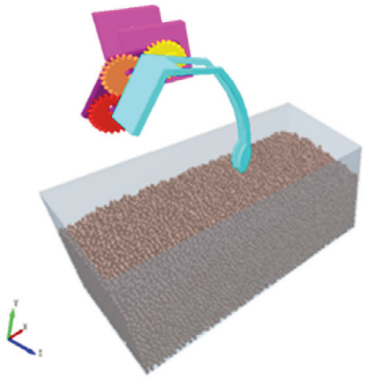

Figure 7. EDEM simulation model.

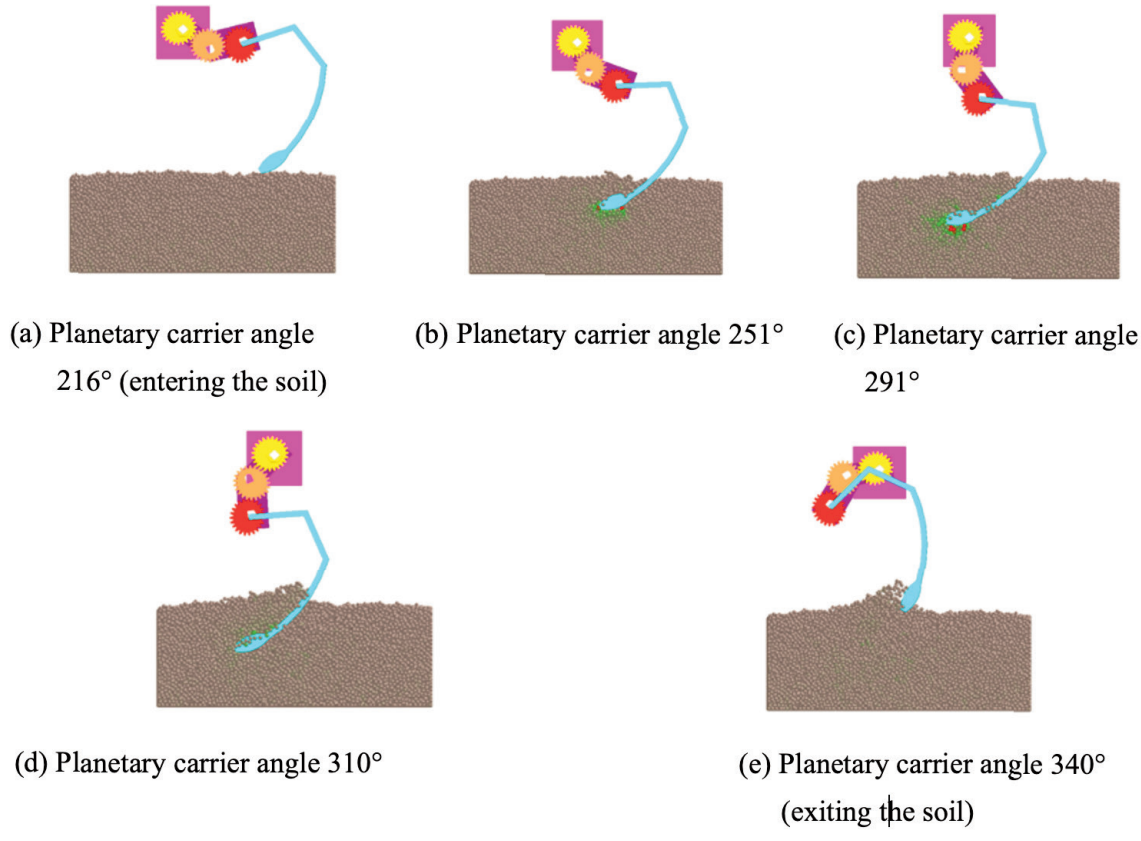

Figure 8. Co-simulation process.

planetary carrier angle range of 216° to 339° (Figure 3) must be considered. According to the working cycle diagram of the transplanting mechanism, this phase involves transplaning, return, and transport processes (Dong *et al*., 2024; Liu *et al*., 2019). Therefore, the force analysis during this phase should incorporate the soil resistance F_x, F_y and soil torque M_S obtained from the previous simulations. Separate dynamic models should be developed for the planetary gear for each of the four stages of the seeding pick-up, transport, transplanting, and return (Kang *et al*., 2025; Twardoch *et al*., 2024).

The force analysis of the planetary gear during the seedling planting stage is shown in Figure 10. The following dynamic equations are established.

$$\sum F_x = F_{Bx} - F_{Jx} - F_{Sx} - \left(F_T + F_{Dx'} - F_H\right)\cos\alpha_1 + \left(F_{KT} + F_{Dy'}\right)\sin\alpha_1 - \left(m_X - m_B - m_T\right)\left[\ddot{x}_B - \ddot{\varphi}_3\left(y_{CX} - y_B\right) - \left(\dot{\varphi}_3 + \dot{\varphi}\right)^2\left(x_{CX} - x_B\right)\right] = 0 \quad \text{(Eq. 1)}$$

$$\sum F_y = F_{By} - F_{Jy} - F_{Sy} - \left(F_T + F_{Dx'} - F_H\right)\sin\alpha_1 - \left(F_{KT} + F_{Dy'}\right)\cos\alpha_1 - \left(m_X - m_B - m_T\right)\left[\ddot{y}_B + \ddot{\varphi}_3\left(x_{CX} - y_B\right) - \left(\dot{\varphi}_3 + \dot{\varphi}\right)^2\left(y_{CX} - y_B\right)\right] - \left(m_X - m_B - m_T\right)g = 0 \quad \text{(Eq. 2)}$$

$$\sum M_B = M_J - M_S - \left(m_X - m_T - m_B\right)g\left(x_{CX} - x_B\right) + F_{Dx'}y'_D - F_{Dy'}x'_D - F_{KT}x'_{CT} + \left(F_T - F_H\right)y'_{CT} - J_X\ddot{\varphi}_3 - \left(m_X - m_T - m_B\right)\left[\ddot{y}_B\left(x_{CX} - x_B\right) - \ddot{x}_B\left(y_{CX} - y_B\right)\right] = 0 \quad \text{(Eq. 3)}$$

where: m_X is the mass of the transplanting arm, m_B is the mass of the fork, m_T is the mass of the push rod, F_T is the force exerted by the spring on the push rod, F_{KT} is the supporting force exerted by the transplanting arm housing on the push rod, F_H is the push rod slide resistance, (F_{Jx}, F_{Jy}) is the meshing force between the planetary gear and the intermediate gear, (F_{Bx}, F_{By}) is the force acting at the rotation center of the transplanting arm, (F_{Sx}, F_{Sy}) is the soil resistance acting on the transplanting arm, M_S is the soil torque acting on the transplanting arm, M_J is the torque transmitted from the intermediate gear to the planetary gear, (F_{Dx}, F_{Dy}) is the force acting at the rotation center of the fork in the relative coordinate system, (x_B, y_B) is the displacement of the rotation center of the planetary gear, $(\ddot{x}_B, \ddot{y}_B)$ is the acceleration of the rotation center of the planet gear, $\dot{\varphi}$ is the angular velocity of the planetary carrier, $\dot{\varphi}_3$ is the relative angular velocity of the planetary gear, $\ddot{\varphi}_3$ is the relative angular acceleration of the planetary gear, (x'_{CT}, y'_{CT}) is the center of mass coordinates of the push rod in the relative coordinate system.

The return phase is divided into two stages: before and after the transplanting arm emerges from the soil. Prior to emergence, the soil resistance and torque acting on the planetary gear gradually decrease. After the arm emerges, these loads cease to act. The force analysis is shown in Figure 11, and the following dynamic equations are established.

$$\sum F_x = F_{Bx} - F_{Jx} - F_{Sx} - m_X\left[\ddot{x}_B - \ddot{\varphi}_3\left(y_{CX} - y_B\right) - \left(\dot{\varphi}_3 + \dot{\varphi}\right)^2\left(x_{CX} - x_B\right)\right] = 0 \quad \text{(Eq. 4)}$$

$$\sum F_y = F_{By} - F_{Jy} - F_{Sy} - m_X g - m_X\left[\ddot{y}_B + \ddot{\varphi}_3\left(x_{CX} - y_B\right) - \left(\dot{\varphi}_3 + \dot{\varphi}\right)^2\left(y_{CX} - y_B\right)\right] = 0 \quad \text{(Eq. 5)}$$

$$\sum M_B = M_J - M_S - m_X g\left(x_{CX} - x_B\right) - J_X\ddot{\varphi}_3 - m_X\left[\ddot{y}_B\left(x_{CX} - x_B\right) - \ddot{x}_B\left(y_{CX} - y_B\right)\right] = 0 \quad \text{(Eq. 6)}$$

The dynamic equations for the planetary gear during the seedling pick-up stage are similar to those during the transplanting stage. However, in this stage, the sliding direction of the push rod is opposite to that of the planting stage, so the slideway resistance term (F_H) in the equations should be reversed. Since the transplanting arm is not subjected to soil resistance during the seedling pick-up process, the corresponding soil resistance and torque terms (*i.e*., F_x, F_y, and M_S) are all set to zero.

The dynamic equations for the planetary gear during the trans-

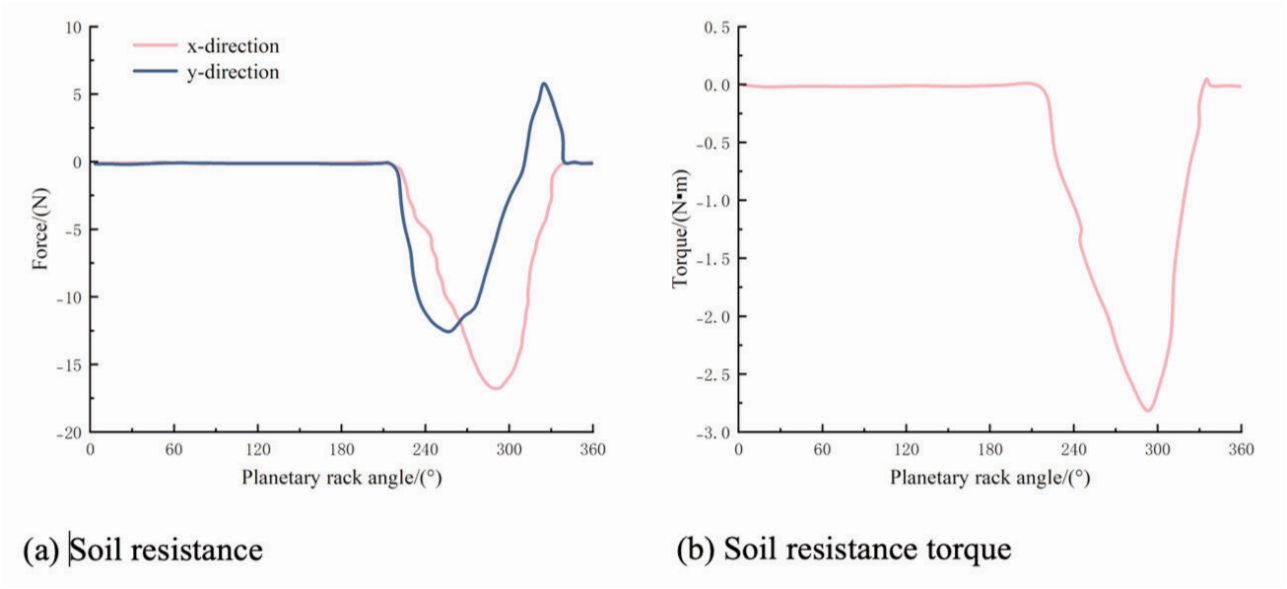

Figure 9. Curve showing changes in the soil resistance and torque on the transplanting arm.

port stage closely resemble those of the return stage. Additionally, the forces and torques (*i.e.*, F_{Nx}, F_{ny}, M_{TB}) exerted by the cam on the fork are incorporated into the equilibrium equations.

Modelling the dynamics of intermediate gears

The force analysis of the intermediate gear is shown in Figure 12. The dynamic equilibrium equation is established.

$$\sum F_x = F_{Ax} - F_{Px} + F_{Jx} - m_Z\left[\ddot{x}_A - \ddot{\varphi}_2(y_{CE} - y_A) - (\dot{\varphi} + \dot{\varphi}_2)^2(x_{CE} - x_A)\right] = 0 \quad \text{(Eq. 7)}$$

$$\sum F_y = F_{Ay} - F_{Py} + F_{Jy} - m_Z g - m_Z\left[\ddot{y}_A + \ddot{\varphi}_2(x_{CE} - x_A) - (\dot{\varphi} + \dot{\varphi}_2)^2(y_{CE} - y_A)\right] = 0 \quad \text{(Eq. 8)}$$

$$\sum M_A = M'_J + M_P - m_Z g(x_{CE} - x_A) - J_Z\ddot{\varphi}_2 - m_Z\left[\ddot{y}_A(x_{CE} - x_A) - \ddot{x}_A(y_{CE} - y_A)\right] = 0 \quad \text{(Eq. 9)}$$

where: (F_{Px}, F_{Py}) is the meshing force between the intermediate gear and the sun gear, (F_{Ax}, F_{Ay}) is the force acting at the rotation center of the intermediate gear, m_Z is the mass of the intermediate gear, $\dot{\varphi}_2$ is the relative angular velocity of the intermediate gear,

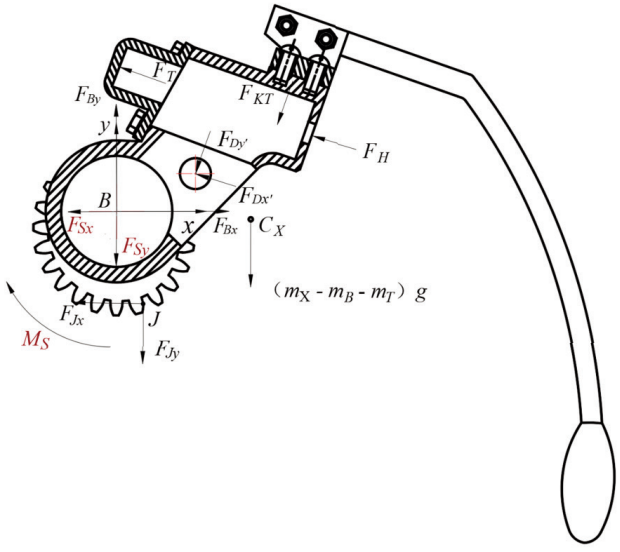

Figure 10. Force analysis diagram of the planetary gear (including the transplanting arm) during the seedling pick-up stage.

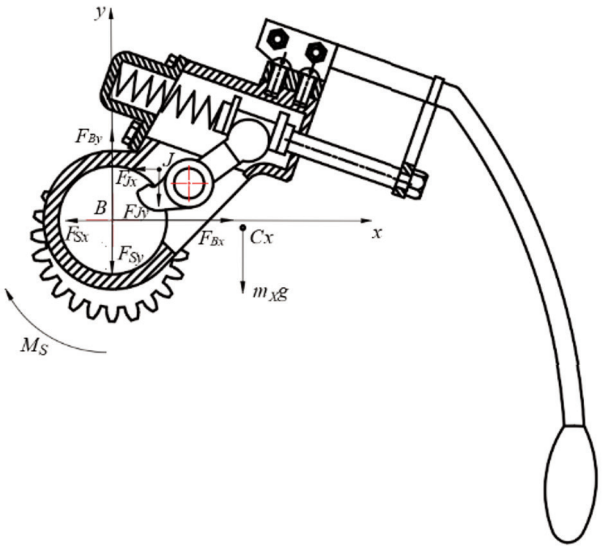

Figure 11. Force analysis diagram of the planetary gear (including the transplanting arm) during the return phase (before excavation).

$\ddot{\varphi}_2$ is the relative angular acceleration of the intermediate gear, (x_A, y_A) is the displacement of the rotation center of the intermediate gear, ($\ddot{x}_A$, $\ddot{y}_A$) is the acceleration of the rotation center of the intermediate gear, M'_j is the torque transmitted from the planetary gear to the intermediate gear, M_P is the torque transmitted from the sun gear to the intermediate gear, J_Z is the moment of inertia of the intermediate gear about its rotation center, (x_{CE}, y_{CE}) is the coordinates of the center of mass of the intermediate gear.

Sun gear dynamics modelling

The force analysis of the sun gear is shown in Figure 13. The dynamic equilibrium equations are established:

$$\sum F_x = F_{O2x} + F_{Px} = 0 \quad \text{(Eq. 10)}$$

$$\sum F_y = F_{O2y} + F_{Py} - m_Y g = 0 \quad \text{(Eq. 11)}$$

$$\sum M_{O2} = M'_P - m_Y g(x_{CY} - x_{O2}) + M_Y = 0 \quad \text{(Eq. 12)}$$

where: m_Y is the mass of the sun gear, (F_{O2x}, F_{O2y}) is the force acting on the sun gear, M_Y is the torque acting on the sun M'_P is the torque transmitted from the intermediate gear to the sun gear.

Planetary carrier dynamics modelling

The force analysis of the planetary carrier is shown in Figure 14. The dynamic equilibrium equations are established:

$$\sum F_x = F_{O1x} - F_{Ax} - F_{Nx} - F_{Bx} - F_L \cos\alpha_L = 0 \quad \text{(Eq. 13)}$$

$$\sum F_y = F_{O1y} - F_{Ay} - F_{Ny} - F_{By} - F_L \sin\alpha_L - m_K g = 0 \quad \text{(Eq. 14)}$$

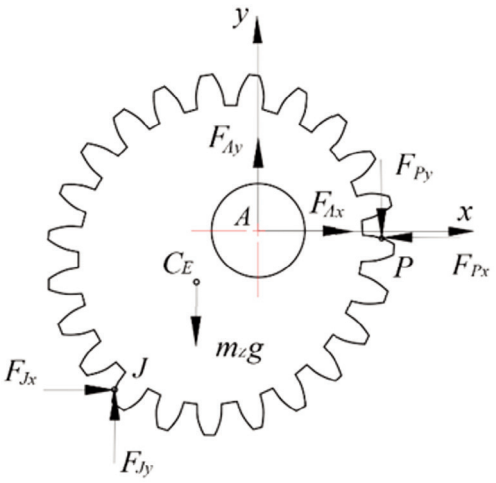

Figure 12. Force analysis diagram of the intermediate gear.

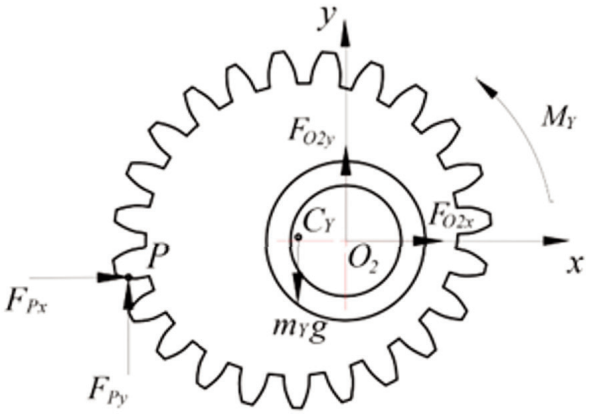

Figure 13. Sun gear analysis diagram.

$$\sum M_{O1} = F_{Ax}y_A - F_{Ay}x_A + F_{Nx}y_B - F_{Ny}x_B + F_{Bx}y_B - F_{By}x_B + M_{BT} - m_K g\, L_8 \cos(\beta_4 + \varphi) + M_L = 0 \quad \text{(Eq. 15)}$$

where: F_{O1x}, F_{O1y} is the force acting at the rotation center of the mechanism, M_{BT} is the reaction torque of the cam, M_L is the driving torque of the mechanism, m_K is the mass of the planetary carrier, L_g is the distance from the center of mass of the planetary carrier to its rotation center.

Frame dynamics modelling

The stress analysis of the frame is shown in Figure 15. The dynamic equilibrium equations are established:

$$\sum F_x = F_{Hx} - F_{O1x} - F_{O2x} = 0 \quad \text{(Eq. 16)}$$

$$\sum F_y = F_{Hy} - F_{O1y} - F_{O2y} - m_J g = 0 \quad \text{(Eq. 17)}$$

$$\sum M_H = (F_{O1x} + F_{O2x})L_9 - M_Y + M_Q = 0 \quad \text{(Eq. 18)}$$

where: (F_{Hx}, F_{Hy}) is the reaction force at the frame, m_J is the mass of the frame, is the torque acting on the frame.

Analysis of the dynamic results

Based on the governing dynamic equations of the modified elliptical gear planetary transplanting mechanism and the sequential solution method, a mechanism dynamics solver was developed using MATLAB. The dynamic responses of the planetary gear components were calculated at a rotational speed of 40r/min, as shown in *Figure S1*.

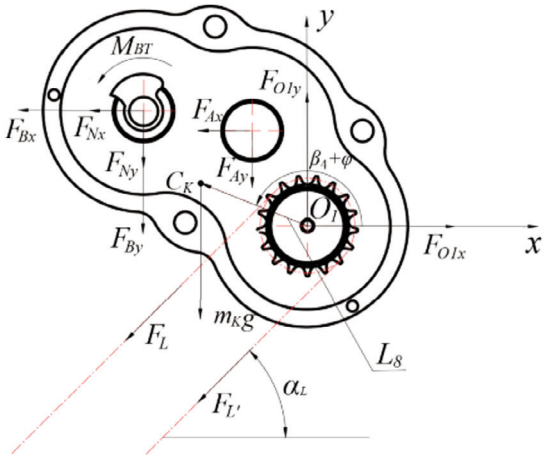

Figure 14. Planetary carrier stress analysis diagram.

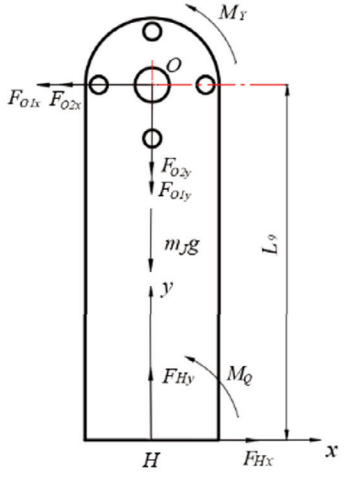

Figure 15. Frame force analysis diagram.

As shown in *Figure S1 a-f*, the force curves of the transmission components in the transplanting mechanism exhibit significant variations during both the seedling pick-up stage (planetary carrier angle between 35° and 108°) and the soil-contact stage (planetary carrier angle between 216° and 339°). These fluctuations arise because the seedling pick-up resistance and the soil resistance during soil penetration are transmitted back to the transmission system through the planetary gears (Zhu *et al*., 2023; Yin *et al*., 2021), causing abrupt changes in the forces acting on the mechanism. Furthermore, as shown in *Figure S1 e,f,* the driving torque of the mechanism and the support reaction force abrupt changes during the transplanting stage (planetary carrier angle from 306° to 309°). This phenomenon results from the rapid rebound of the transplanting arm's push rod, which triggers the gripping claws to release the sweet potato seedlings, thereby generating significant impact and vibration within the mechanism.

Transplanting mechanism dynamics test

Dynamic test plan

To investigate the dynamic characteristics of the sweet potato seedling transplanting mechanism prototype, a dynamic test bench and its three-dimensional model were designed and constructed, as shown in *Figure S2*, to measure the support reaction force and driving torque. During the test, the motor speed was set to 40 r/min. The CL-YD-3301 three-axis force sensor (2), mounted on the force sensor pad (3), converted the support reaction force into an electrical signal. This signals were subsequently filtered and amplified by the MI2004 signal amplifier (13) before being transmitted to the data acquisition instrument (12). The data acquisition and analysis software processed and analyzed the time-varying support reaction force data. The JN-DN1 dynamic torque sensor (6), connected via couplings to the motor output shaft (8) and the chain drive input shaft (14), transmitted the measured driving torque signal to the MCK-DN dynamic torque measurement and control instrument (11). The processed data were subsequently imported into a computer for comprehensive analysis.

Analysis of the dynamic test results

Dynamic tests of the sweet potato seedling transplanting mechanism were conducted at a speed of 40 r/min to obtain the variation curves of the driving torque and support reaction force. After filtering the measured data, and the resulting curves are shown in *Figure S3*. Additionally, the mean and variance of both the experimental results from the dynamic test bench and the theoretical analysis were calculated, as shown in *Table S3*.

Comparing the experimental curve (*Figure S3*) with the theoretical prediction curves (*Figure S1 e,f*) of the transplanting mechanism reveals a high degree of consistency in their variation trends. Combined with the data analysis in Table S3, the measured load mean and peak values are slightly higher than the theoretical calculations due to friction resistance and transmission losses. For example, the torque peak (2.10 N·m) is slightly higher than the theoretical value (1.43 N·m). Simultaneously, due to the chain polygon effect, mechanism installation errors, machining tolerances, and discrepancies between actual soil resistance and simulated loads, the experimental curve exhibits noticeable nonlinear fluctuations with significant variance. Despite these numerical deviations, the overall error remains within reasonable engineering limits, validating the effectiveness of this dynamic model in characterizing the actual force state of the mechanism and providing reliable basis for subsequent structural optimization.

Conclusions

This study analysed the dynamics of a sweet potato seedling transplanter by combining ADAMS-EDEM co-simulation with experiments. An accurate model was established to reveal soil-machine interactions and was validated through testing. This work provides a practical basis for structural design and optimization. The main conclusions are as follows:

i) Based on the working principle of the sweet potato seedling transplanting mechanism, dynamic simulation models of the mechanism and discrete element models of the soil were established using ADAMS and EDEM, respectively. An ADAMS-EDEM co-simulation was conducted to analyze the interaction between the mechanism and the soil, yielding the soil resistance variation curve acting on the transplanting arm. This approach effectively addressed the difficulty of quantifying soil resistance, providing a solid foundation for establishing a dynamic model of the transplanting mechanism.

ii) Based on the force transmission relationships within the sweet potato seedling transplanting mechanism, the force conditions of each component in the planetary gear system were analyzed. A kineto-static analysis method was employed to establish a dynamic model of the transplanting mechanism incorporating soil resistance. Subsequently, dynamic analysis software was developed on the MATLAB platform to obtain force curves for each component in the planetary gear system. The dynamic characteristics of the transplanting mechanism were then thoroughly analyzed.

iii) Dynamic experiments were conducted on the sweet potato seedling transplanting mechanism, yielding experimental curves for support reaction forces and driving torques. Bench test comparisons validated the accuracy and reliability of the proposed dynamic theoretical model. This research facilitates the numerical assessment of dynamic loads acting on critical components, establishing representative load inputs for fatigue-resistant design and lightweight topology optimization. Furthermore, the driving torque profiles establish a theoretical foundation for power matching and motor selection, offering direct engineering guidance to enhance the operational reliability and dynamic performance of the transplanting mechanism.

References

Dong C, Li L, Liu Y, Wei Y, 2024. Translation torsion coupling dynamic modeling and nonlinearities investigation of non-circular planetary gear systems. Nonlinear Dynam 112:18931-18948.

Guo Q, Huihuang X, 2023. A review of the discrete element method/modelling in agricultural engineering. J Agric Eng 54:1534.

Hui L, Tengfei H, Hu L, et al., 2023. Development of a contour-following plug-in transplanting machine for sweet potatoes on film in hilly and mountainous areas. Int J Agric Eng 39:26-35.

Issa IIM, Zhang Z, Yang X, Wang HY, El-Kolaly W, 2020. Design, ANSYS analysis and performance evaluation of potato digger harvester. Int Agric Eng J 29:60-73.

Jun ZHU, Leung AK, Yu W, 2024. A computationally-efficient finite-element model for solving root–soil mechanical interaction of complex root system architectures. Comput Geotech 174:106604.

Jin X, Zhao G, Li M, Li S, Zhou L, Liang J, et al., 2025.

Optimization of transplanting mechanism working parameters based on a coupled machine-soil-pot seedling model. Comput Electron Agr 238:110786.
Kang J, Tian S, Liu S, Liu J, Fu Y, Wang H, Awais M, 2025. Motion analysis and structural parameter optimization for nested multi-link transplanting mechanism of variable plant spacing transplanting machine. PLoS One 20:e0337811.
Lai Q, Yu Q, Dong J, 2019. Dynamic analysis of rotary tiller gearbox based on EDEM, ADAMS and ANSYS. J Intell Fuzzy Syst 36:1153-1160.
Li B, Liu M, Sun P, Zang X, 2023. Research on the operation resistance of bulldozers based on joint simulation technology. J Phys Conf Ser 638:012003.
Li J, Xie S, Liu F, Guo Y, Liu C, Shang Z, Zhao X, 2022. Calibration and testing of discrete element simulation parameters for sandy soils in potato growing areas. Appl Sci 12:101251.
Liu Y, Wang J, Dong C, Wang F, 2025. Mathematical model and kinematic characterisation of a non-circular planetary gear system. T Famena 49:111-128.
Lu H, Wang B, Wang G, Yu Z, You Z, Hu Z, et al., 2016. Design and testing of the 2ZGF-2 sweet potato double-row planting machine. T Chin Soc Agric Machin 32:8-16.
Massah J, Fard MR, Aghel H, 2021. An optimized bionic electro-osmotic soil-engaging implement for soil adhesion reduction. J Terramechan 95:1-6.
Walunj A, Chen Y, Tian Y, Zeng Z, 2023. Modeling soil–plant–machine dynamics using discrete element method: a review. Agronomy 15:1260.
Rajendran M, Ranganathan T, 2025. Advancements in paddy transplanter mechanization implications for sustainable agriculture. Sustain Futures 10:101235.
Sanborn G, Choi J, Choi JH, 2021. Strategy for co-simulation of multi-flexible-body dynamics and the discrete element method. J Mech Sci Technol 35:4363-4380.
Shao Y, Zhang H, Xuan G, Zhang T, Guan X, Wang J, 2023. Simulation and experiment of a transplanting mechanism for sweet potato seedlings with "boat-bottom" transplanting trajectory. Int J Agric Biol Eng 16:96-101.
Shi J, Hu J, Li J, Wei L, Yue R, 2024. Design and experiment of planting mechanism of automatic transplanter for densely planted vegetables. Agriculture 14:1357.
Sun Y, Chen E, Shi L, 2025. Study on the seed metering performance of potato seed metering device with three claw type on DEM. J Agric Eng 56:1902.
Twardoch K, Sierociński D, 2024. An analytical approach to gear mesh dynamics for the sustainable design of agricultural machinery drive systems. Sustainability 17:1837.
Xue K, GaoK, Kuang F, Zhang S, Liao J, Zhu D, 2022. Machinery-plant-paddy soil coupling model based numerical simulation method of mechanical transplanting process of big rice seedling. Comput Electron Agr 198:107053.
Yan W, Hu M, Li K, Wang J, Zhang W, 2022. Design and experiment of horizontal transplanter for sweet potato seedlings. Agriculture 12:675.
Ye B, Wu G, Yu G, Jin X, Liang S, 2016. Optimisation design and experiment of a non-circular gear planetary gear system for rice seedling transplanting mechanism. T Chin Soc Agric Machin 47:68-73.
Ye B, Hao Z, Gaohong Y, et al. 2016. Kinematic analysis and experiment of a rotary rice seedling transplanting mechanism. T Chin Soc Agric Machin 47:53-61.
Ye B, Li L, Gaohong Y, et al., 2014. Kinematic analysis and experiment of a rotary seedling picking mechanism for vegetable pots. T Chin Soc Agric Machin 45:70-78.
Ye B, Tang T, Yu G, et al., 2018. Kinematic analysis and experiment of a combined non-circular gear planetary gear train sampling mechanism. T Chin Soc Agric Machin 49:74-82.
Ye B, Ye Y, Zhou H, Yu G, Zhao X, Deng B, 2024. Design and experimental research on the sweet potato seedling transplanting mechanism of the planetary gear train with deformed elliptical gear transmission. Int J Agric Biol Eng 17:91-99.
Yin J, Wang Z, Zhou M, Wu L, Zhang Y, 2021. Optimized design and experiment of the three-arm transplanting mechanism for rice potted seedlings. Int J Agric Biol Eng 14:56–62.
Yu S, Song X, Sun Z, 2023. On-line prediction of resistant force during soil–tool interaction. IFAC-Pap 56;133-138.
Zhang L, Zhai Y, Chen J, Zhang Z, Huang S, 2022. Optimization design and performance study of a subsoiler underlying the tea garden subsoiling mechanism based on bionics and EDEM. Soil Tillage Res 220:105375.
Zhou M, Yang J, Xu T, Ying J, Wang X, 2022. Optimal design of transplanting mechanism with differential internal engagement non-circular gear trains. J. Agric. Eng. 53:1412.
Zhou H, Mengying Y, Hongbin X, et al., 2025. Design and experiment of an elliptical gear planetary gear system for sweet potato transplanting mechanism. J Zhejiang Univ Tech (Natural Science).53:96-104.
Zhu D, Gao K, Xue K, Zhang S, Liao J, Wang T, et al., 2023. Vibration analysis and parameter optimization of seedling pushing device of transplanting mechanism with planetary elliptic gears. J Chin Inst Eng 46:154-162.

Online Supplementary Material
Figure S1. Results of the dynamic analysis of the planetary gear system.
Figure S2. Transplanting mechanism dynamics test bench and its three-dimensional model.
Figure S3. Dynamic test results of the transplanting mechanism prototype.
Table S1. Related parameters for the soil.
Table S2. Soil simulation angle of repose under different surface energy parameters.
Table S3. Comparison of institutional prototype dynamic test bench test results and theoretical analysis results.

Received: 30 July 2025; Accepted: 6 March 2026.

Contributions: Bingliang Ye: conceptualization, methodology, software, investigation, writing – original draft, writing – review & editing. Hongbin Xue: methodology, formal analysis, visualization, writing – review & editing. Gaohong Yu: supervision, validation, writing – review & editing. Yuxuan Ye: Software, Methodology. Haili Zhou: investigation, writing – review & editing.
Conflict of interest: the authors declare that there are no conflicts of interest regarding the publication of this paper.

Availability of data and materials: the datasets used and/or analyzed during the current study are available from the corresponding author on reasonable request.

Acknowledgements: this work was supported by the Zhejiang Provincial Natural Science Foundation of China (LD24E050007) and the National Natural Science Foundation of China Project (32171899, 32201676).